

Construction of Reversible Lattice Molecular Automata

Takayuki Nozawa and Toshiyuki Kondo

tknozawa@cc.tuat.ac.jp

Abstract

Several cellular automata (CA) models have been developed to simulate self-organization of multiple levels of structures. However, they do not obey microscopic reversibility and conservation laws. In this paper, we describe the construction of a *reversible lattice molecular automata* (RLMA) model, which simulates molecular interaction and self-organization of higher-order structures. The model's strict reversibility entails physically relevant conservation laws, and thus opens a way to precise application and validation of the methods from statistical physics in studying the necessary conditions for such multiple levels of self-organization.

Keywords: Reversible Cellular Automata; Molecular Aggregation; Self-organization; Artificial Chemistry

1 Introduction

Possessing and utilizing multiple levels of self-organized structures—sometimes addressed as *dynamical hierarchies*[1, 2]—is a characteristic feature of biological systems. Cellular automata (CA) and similar discrete paradigms have been effective in modeling such dynamical self-organization hierarchies. In the context of molecular aggregation, *lattice molecular automata* (LMA) simulates self-organization of water (polar solvent), monomers, and polymers into clusters and higher-order structures such as micelles[3, 4, 5], and similar models have been developed to simulate organization of compartment structure and proto-cell-like self-reproduction[6, 7].

However, these models do not obey microscopic *reversibility* and conservation laws, and therefore, the possibility and stability of the self-organized structures in these models are, to some extent, implied in their irreversible time evolution rules. Under the laws of physics, stable persistence of an organized structure requires effective utilization of limited resources and smooth disposal of generated entropy. Therefore, the constraint of reversibility should not be omitted in studying the necessary conditions for stable structures, using, for example, the canonical methods of statistical physics.

In this paper, we describe the construction of *reversible lattice molecular automata* (RLMA), which simulates self-organization of water, monomers, and polymers with a strictly reversible dynamics and physically appropriate conservation laws. Although several reversible CA models have been proposed to simulate self-organization processes[8, 9], our model can simulate self-organization of structures with *mobility*, which will be essential for realizing higher-order structures and higher functionality such as autonomy.

The rest of the paper is organized as follows. A formal definition of CA is provided and useful techniques in constructing reversible CA are briefly reviewed in Section 2. Features of the original LMA model and its relation to other models are also briefly reviewed there. The construction of our RLMA model is described in Section 3, along with the conservation laws derived from the reversible dynamics. Some simulations of monomers and polymers in polar solvent are presented in Section 4. Finally, our conclusion is drawn in Section 5. Appendix A presents an alternative approach for implementing reversible molecular rotation.

2 Preliminaries

2.1 Formalization of CA

On a d -dimensional spatial lattice \mathbb{Z}^d , each site (cell) $\mathbf{i} \in \mathbb{Z}^d$ is assigned with its *local state* $\omega_{\mathbf{i}} \in A$. The finite set A of local states is called an *alphabet*. A specification of local states over the whole space $\omega \triangleq (\omega_{\mathbf{i}})_{\mathbf{i} \in \mathbb{Z}^d} \in \Omega = A^{\mathbb{Z}^d}$ is called a *global state* or *configuration*.

The dynamics of a CA is given by the *local transition map* φ as

$$\omega_{\mathbf{i}}^{t+1} = \varphi((\omega_{\mathbf{j}}^t)_{\mathbf{j} \in \mathcal{N}(\mathbf{i})}), \quad (1)$$

where the *neighbor function* $\mathcal{N} : \mathbf{i} \mapsto (\mathbf{j}_1, \dots, \mathbf{j}_N)$ defines interaction range for each site \mathbf{i} . By applying the local map φ over the lattice, the *global transition map*

$$\omega^{t+1} = \Phi(\omega^t) \quad (2)$$

from a configuration at t to the one at $t + 1$ is derived. Although the application of φ over the space is synchronous in simple CA, making it asynchronous can be effective in satisfying reversibility and other constraints, as shown later. Furthermore, in more complicated CA, the local map φ consists not of a single map but of several maps (sub-steps), and the local states $\omega_{\mathbf{i}} \in A$ also have inner structures such as “partitions” or “layers.”

When the global transition map Φ is bijective, that is, when for any configuration ω^{t+1} its pre-image ω^t is unique, the CA is *reversible* (or *invertible*).

2.2 Construction of reversible CA

Reversibility entails *conservation of information*—differences in states cannot just appear from or vanish into nowhere. Hence the manner in which to prevent

information loss is crucial in constructing reversible CA.

Since the many-to-one local transition map φ in Eq. (1) obviously loses information by itself (Fig. 1(a)), the loss should be prevented by well-counterbalanced distribution among the interacting cells. However, designing such maps is far from trivial. Indeed, judging the reversibility of a global transition map Φ , given its corresponding local map φ , is a difficult task in itself.

An easier method to construct reversible CA is by adopting a *permutation* (reversible transformation on a finite set) ψ ,

$$\psi : A^B \rightarrow A^B, \quad (3)$$

instead of a many-to-one mapping φ , as a constituent of the transition rule (Fig. 1(b)). Here, B denotes a “block” of cells under the permutation. In *Partitioning CA* (or *block CA*) [10], for example, both the reversibility and global transmission of information are satisfied by combining the permutation and alternation of different partitioning schemes of a given space into cell-blocks.

The permutation (3) can be generalized into a *conditional permutation* as

$$\psi_c : A^S \rightarrow A^S, \quad c \in A^C. \quad (4)$$

Out of the set $C + S$ of cells that are subject to the mapping, the states of cells in C work as “control signals,” which determine a permutation for the states of S , and reappear unchanged as outputs (Fig. 1(c)). The Fredkin gate and the Toffoli gate are well-known examples of conditional permutations.

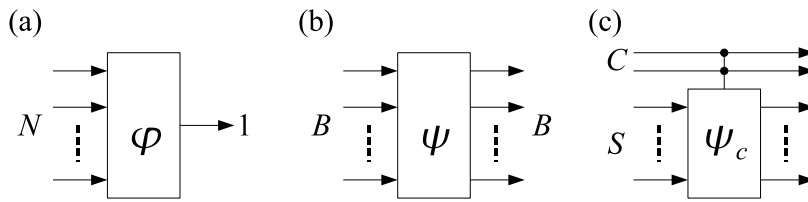


Figure 1: Mappings to constitute transition: (a) many-to-one mapping, (b) permutation, and (c) conditional permutation.

To prevent information loss, the outputs of the (conditional) permutations should be reused as inputs or conditional signals, and to achieve this, one needs to implement certain techniques such as dividing a time step into several *sub-steps*, and arranging the permutations *sparingly and asynchronously in space-time* [11].

For synchronous information transmission, one can also use global *shifts*, which uniformly displace some partitions or layers of local states. The translational movement of free particles can be effectively modeled by the shifts. In *lattice gas automata* (LGA) [12, 13], for example, shifts are utilized to express the translation of gas particles, in combination with permutations that represent the collisions of the particles. *Partitioned CA* [14] is virtually equivalent to the LGA.

2.3 LMA model and other models

Various models have been proposed and used to simulate molecular self-organization processes. On the one hand, the molecular dynamics (MD) method models molecules as particles with appropriate interaction potentials, and solves their equations of motion in continuous space[15]. While the MD enables microscopically detailed description of the dynamics, size of the simulated system is restricted by the available computer resources. On the other hand, lattice-type models have been successful on simulating macroscopic behavior of phase separation and aggregation processes. Especially the Larson model[16, 17, 18] and its variants[19, 20, 21, 22] are widely used and many results are reported. In the traditional Larson model simulating ternary mixture of water, oil (hydrophobic monomers), and surfactant (amphiphilic polymers), water and hydrophobic monomers are represented by a set of up and down (+1, -1) spins, respectively, and polymers are represented by strings of spins. Monte Carlo method is used for update and the ferromagnetic interaction between the spins induces phase separation, micelle formation, etc.

The original LMA model bridges the gap between the MD method and the Larson-type models[5]: While realized in a discrete manner and thus keeping the efficiency of the lattice setting, it includes some microscopic molecular details, such as hydrodynamics conserving momenta in the molecular collision, directions of polar molecules and accompanied anisotropy of molecular potential energy. A distinguishing feature of the LMA model is the equienergetic interaction for the pairs water-hydrophobic monomer and hydrophobic monomer-hydrophobic monomer, following experimental data on enthalpy exchanges in mixtures[23]. This setting is in contrast to the Larson models, which define positive enthalpic gains for oil-oil interaction but not for water-oil interaction. Consequently, in the LMA model phase separation is realized via *entropy-driven* hydrophobic effect, and not enthalpy-driven as in the Larson-type models.

Although update rule of the LMA model partially keeps the conservation laws, its dynamics is not microscopically reversible (refer to section IV.B and V of Ref. [3] for example to see the total energy is conserved in the mean but not strictly and explicitly). Therefore, utilizing the techniques introduced in section 2.2, we construct our RLMA model in the next section.

3 RLMA Model

3.1 Space

We formalize the RLMA model on the two-dimensional triangular lattice (Fig. 2(a), (b)) as in the literature[3, 4], although generalization to other lattice structures and to higher dimensions will be straightforward. We use the variable $l \in \{+1, +2, +3, -1, -2, -3\} \equiv L$ to denote the principal directions, and $l(i)$ to denote cell i 's nearest neighbor in direction l , as shown in Fig. 2(c). L corresponds to $\{0, \pi/6, \dots, 5\pi/6\}$ in the equilateral triangular lattice with a proper coordinate system (Fig. 2(c)), and on L , we define a cyclic permutation Δ of

length 6,

$$\Delta = \begin{pmatrix} +1 & +2 & +3 & -1 & -2 & -3 \\ +2 & +3 & -1 & -2 & -3 & +1 \end{pmatrix}, \quad (5)$$

which corresponds to $+\pi/6$ rotation operator for the principal directions.

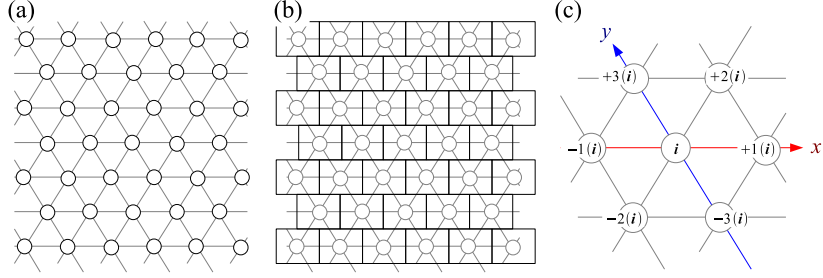


Figure 2: Two-dimensional triangular lattice: (a) structure, (b) corresponding cells, and (c) principal directions and nearest neighbors.

3.2 Local states

Each local state has the *layers* (internal data structure) shown in Table 1.

Table 1: Structure of local states.

Layer name and variable	Values
Molecular type mt_i	Water (W), hydrophilic monomer (I), hydrophobic monomer (O), or vacuum (V)
Molecular orientation mo_i	$mo_i \in L$ for polar molecules, $mo_i = \mathbf{null}$ otherwise
Translational kinetic energy $(tke_{i,l})_{l \in L}$	$tke_{i,l} \in \{0, 1\}$ for molecules, while non-zero values in the opposing directions are forbidden
Rotational kinetic energy rke_i	$\{-1, 0, +1\}$ (polar: $\{\pm 1\}$, non-polar: 0)
Molecular bonds $(mb_{i,l})_{l \in L}$	Up to two bonds for hydrophilic or hydrophobic monomers
Heat particles $(h_{i,l})_{l \in L}$	$h_{i,l} \in \{0, \dots, H_{\max}\}$ for each $l \in L$
Preferential direction pd_i	$pd_i \in L$

For each cell $i \in \mathbb{Z}^2$, *molecular type* mt_i takes one of three types of molecules—*water* (W), *hydrophilic monomer* (I), *hydrophobic monomer* (O), or *vacuum* (empty; V). For example, one can consider the hydrophilic monomer to be acetic acid and the hydrophobic monomer to be methane. A site can contain at most one molecule; this constraint corresponds to *excluded volume*.

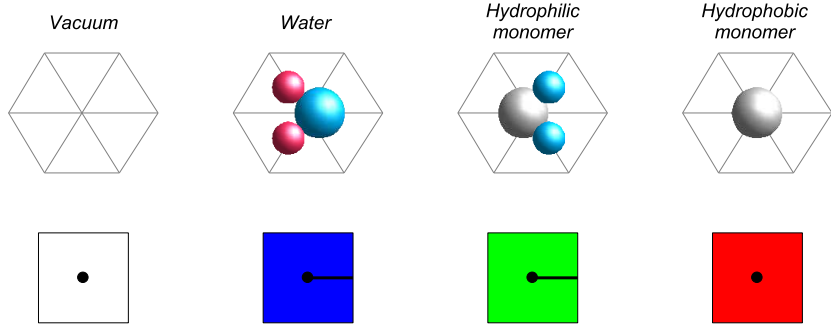


Figure 3: Molecular types. Upper row: schematic illustrations. Lower row: representations in visualization of the simulation results; bars indicate the orientations of polar molecules.

Water and hydrophilic monomers are polar molecules; therefore, they have *molecule orientation* $mo_i \in L$. (For hydrophobic monomers and vacuum, $mo_i = \text{null}$.) We define that, for water in orientation mo , the same direction represents negative polarization (corresponding to one oxygen) and $\Delta^{\pm 2}(mo)$ represents positive polarization (corresponding to two hydrogens), and for a hydrophilic monomer in orientation mo , $\Delta^{\pm 1}(mo)$ represents negative polarization (corresponding to O or OH) (See Fig. 3). Molecular orientation affects the strength of *potential energy* induced by several kinds of molecular interaction (see section 3.3).

The sites occupied by molecules have *translational kinetic energy* (TKE) $the_{i,l} \in \{0, 1\}$ in every principal direction $l \in L$, although non-zero energy values in opposite directions on the same line are forbidden ($the_{i,l} + the_{i,-l} \leq 1$). Hence, there are 27 possible TKE states for a molecule (Fig. 4).

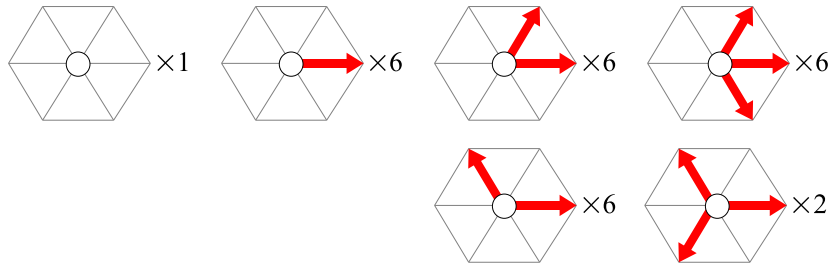


Figure 4: Possible states of translational kinetic energy for a molecule.

Molecules can have *rotational kinetic energy* (RKE) rke_i , which allows the rotation of the polar molecules to be reversible (see section 3.4.4). For proper

update by the rotation rule given here, we confine the value of rke_i to $\{+1, -1\}$ for polar molecules, and to zero for non-polar molecules or vacuum. (For an alternative setting, see Appendix A.)

Hydrophilic and Hydrophobic monomers can have *molecular bonds* with neighboring monomers. We define that

$$mb_{i,l} = \begin{cases} 1 & \text{if two monomers at } i \text{ and } l(i) \text{ are bonded,} \\ 0 & \text{otherwise.} \end{cases} \quad (6)$$

(Thus, $mb_{i,l} = mb_{l(i),-l}$.) *Polymers* can be composed as a group of monomers linked by the bonds, as shown in Fig. 5. In the current study, we suppose that for each monomer to have the bonds in at most two directions, $\sum_{l \in L} mb_{i,l} \leq 2$; thus, the polymers are one-dimensional. One can consider the polymers to be fatty acids.

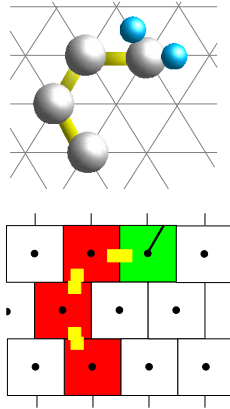


Figure 5: Schematic representation of a polymer.

For the above layers, which are related to molecules, we also overlay the *heat particles* layer on each cell. The heat particle variable $h_{i,l}$ can take values of $\{0, \dots, H_{\max}\}$ independently for every direction $l \in L$.

Finally, we append the *preferential direction* $pd_i \in L$ for each cell i . In the transition rule given below, the preferential direction works as a “fluctuation” to break irreversibility-inducing symmetry. The *parity* of the preferential direction, defined by

$$\text{parity}(pd_i) = \begin{cases} +1 & \text{if } pd_i \in \{+1, +3, -2\}, \\ -1 & \text{if } pd_i \in \{+2, -1, -3\}, \end{cases} \quad (7)$$

is also utilized in the transition rule.

Molecular type, orientation, TKE and, molecular bonds (or variables equivalent to them) are included in the original LMA[4, 5]. On the other hand, RKE, heat particles, and preferential direction are introduced in this model to implement reversibility in a physically appropriate manner.

3.3 Potential energy

Every molecule interacts with its nearest neighboring molecules;¹ therefore, it has *potential energies* for each of the six principal directions. In calculating potential energy, we consider only pairwise interactions, and let $V^{i,l(i)}$ denote potential energy arising from the interaction between molecules at i and $l(i)$. The molecular interaction is divided into three classes:²

- Electrostatic interactions between permanent multipoles, which take place when the polarized directions of the two polar molecules face each other. Let $V_{\text{perm-perm}}$ represent the potential energy contribution from this class of interactions.
- Induction-based interactions between a permanent multipole and an induced multipole, which take place when a polarized direction of one molecule faces an originally non-polarized direction of another. Let $V_{\text{perm-ind}}$ represent the potential energy contribution from this class of interactions.
- London dispersion interactions between induced multipoles, which take place when the surfaces of two non-polar molecules face each other. Let $V_{\text{ind-ind}}$ represent the potential energy contribution from this class of interactions.

Then, the total potential energy in the system is calculated as

$$V_{\text{total}} = \frac{1}{2} \sum_i \sum_{l \in L} V^{i,l(i)} = \frac{1}{2} \sum_i \sum_{l \in L} \left(V_{\text{perm-perm}}^{i,l(i)} + V_{\text{perm-ind}}^{i,l(i)} + V_{\text{ind-ind}}^{i,l(i)} \right). \quad (8)$$

For the full specification of the potential terms in our model, the integer parameters listed in Table 2 must be given.

3.4 Transition rule

In the original LMA model, each unit-time update consists of the following sub-steps[4]:

1. propagation of the molecular type and redistribution of kinetic energies,
2. construction of type-specific force fields,
3. calculation of potential energies,
4. calculation of the most proper move direction,
5. readjustment of bonds in polymers according to the move direction, and
6. movement of the molecule and clearing of the old lattice position.

¹Although wider range of interaction can also be modeled, it requires larger number of *site groups* and more complicated update schemes (see section 3.4).

²We omit cooperativity effects because of their minor influence on the simulation results.

Table 2: Parameters of potential energy. Potentials of other neighboring directions of molecular pairs are set to 0.

Class	Potential	Applied cases
$V_{\text{perm-perm}}$	$V_{\text{WH-WH}}$	Where positively polarized directions (Hs) of two water molecules (Ws) face each other
	$V_{\text{WO-WO}}$	Where negatively polarized directions (Os) of two Ws face each other
	$V_{\text{WH-WO}}$	Where an H and an O of two Ws face each other
	$V_{\text{WH-IP}}$	Where an H of a W faces a negatively polarized direction (O or OH) of a hydrophilic monomer (I)
	$V_{\text{WO-IP}}$	Where an O of a W faces a negatively polarized direction of an I
	$V_{\text{IP-IP}}$	Where two negatively polarized directions of two Is face each other
$V_{\text{perm-ind}}$	$V_{\text{WH-WN}}$	Where an H and a non-polarized direction of two Ws face each other
	$V_{\text{WH-IN}}$	Where an H of a W faces a non-polarized direction of an I
	$V_{\text{WH-O}}$	Where an H of a W faces any one of directions of a hydrophobic monomer (O)
	$V_{\text{WO-WN}}$	Where an O and a non-polarized direction of two Ws face each other
	$V_{\text{WO-IN}}$	Where an O of a W faces a non-polarized direction of an I
	$V_{\text{WO-O}}$	Where an O of a W faces any one of directions of an O
	$V_{\text{IP-WN}}$	Where a negatively polarized direction of an I faces a non-polarized direction of a W
	$V_{\text{IP-IN}}$	Where a negatively polarized direction and a non-polarized direction of two Is face each other
	$V_{\text{IP-O}}$	Where a negatively polarized direction of an I faces any one of directions of O
$V_{\text{ind-ind}}$	$V_{\text{O-O}}$	Where any directions of two Os face each other

Although stated otherwise in Ref. [5], many of these sub-steps are irreversible in actuality, involving erasure and duplication of information. To realize reversibility, therefore, we reconstruct the sub-steps and create new ones, utilizing the techniques introduced in section 2.2.

3.4.1 Molecular translation, collision, and excluded volume

In the LMA, for each molecule, the most proper move direction is calculated based on its TKEs and potentials, and the molecule moves to the direction if the movement satisfies the constraints of excluded volume and molecular bond maintenance. This rule causes situations whose pre-images are not unique (*e.g.*, a molecule at a site might have come from one of the neighboring sites according to the most proper move direction, or might have been at the same site a unit time ago because of the constraints), and thus it is irreversible.

To satisfy the constraints of excluded volume and molecular bond maintenance, and to realize reversibility at the same time, we introduce *site groups*. Sites in each group should be scattered uniformly and sparsely enough (to prevent interference of the pairwise interactions defined below, the sites in each group should be separated by at least four times the unit distance). We determine the group to which site \mathbf{i} belongs at time t by the following map

$$g(\mathbf{i}, t) = \{4(i_x \bmod 4) + (i_y \bmod 4) + t\} \bmod 16, \quad (9)$$

and let $G = \{0, 1, \dots, 15\}$ denote the range of g . Here (i_x, i_y) are the coordinates of site \mathbf{i} given by the axis in Fig. 2(c), and each site is assigned to a group, as shown in Fig. 6.

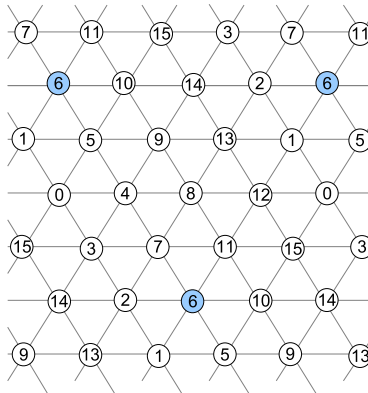


Figure 6: Site groups for interleaved interaction. Sites in the group indexed “6” are shaded.

Using the site groups and the preferential directions, molecular translation and collision are performed in an interleaved manner using the scheme shown in Fig. 7.

```

begin
for  $g$  in site groups  $G$  do
  for  $k$  in  $(0, 1, \dots, 5)$  do
    for every  $i$  in a group  $g$  do
       $j := pd_i(i)$ ;
      if  $\Delta^k(pd_j) = pd_i$  then
         $\psi_{\text{mtc}}(\omega_i, \omega_j)$ ; //pairwise interaction between  $i$  and  $j$ .
      end
    end
  end
end

```

Figure 7: Interleaved paired site interaction scheme. Note Eq. (5) for the definition of Δ .

For the interaction between paired neighboring sites i and $j = pd_i(i)$ in Fig. 7, we define a composite conditional permutation ψ_{mtc} , which represents molecular translation and collision.

When both sites are vacuum, no interaction takes place:

$$mt_i = mt_j = V \Rightarrow \psi_{\text{mtc}}(\omega_i, \omega_j) = (\omega_i, \omega_j) \text{ (identity)}. \quad (10)$$

When i is occupied by a molecule and j is vacuum, the molecule at i moves to j if the TKE in this direction pd_i is positive, or the molecule's TKE in this direction is inverted if the TKE in the opposite direction is positive, or no change takes place if the molecule's TKEs are zero in both directions:

$$\left\{ \begin{array}{l}
\psi_{\text{mtc}} \left(\left(\begin{array}{c} mt_i \\ mo_i \\ (tke_{i,l})_l \\ rke_i \\ (mb_{i,l})_l \end{array} \right), \left(\begin{array}{c} mt_j \\ mo_j \\ (tke_{j,l})_l \\ rke_j \\ (mb_{j,l})_l \end{array} \right) \right) = \left(\left(\begin{array}{c} mt_j \\ mo_j \\ (tke_{j,l})_l \\ rke_j \\ (mb_{j,l})_l \end{array} \right), \left(\begin{array}{c} mt_i \\ mo_i \\ (tke_{i,l})_l \\ rke_i \\ (mb_{i,l})_l \end{array} \right) \right) \\
\psi_{\text{mtc}}(tke_{i,pd_i}, tke_{i,-pd_i}) = \begin{array}{l} (tke_{i,-pd_i}, tke_{i,pd_i}) \\ \text{if } (tke_{i,pd_i}, tke_{i,-pd_i}) = (1, 0), \\ (tke_{i,pd_i}, tke_{i,-pd_i}) \\ \text{if } (tke_{i,pd_i}, tke_{i,-pd_i}) = (0, 1), \\ \end{array} \\
\psi_{\text{mtc}}(\omega_i, \omega_j) = \begin{array}{l} (\omega_i, \omega_j) \\ \text{if } (tke_{i,pd_i}, tke_{i,-pd_i}) = (0, 0). \end{array}
\end{array} \right. \quad (11)$$

(Here, internal layers that are unaffected by ψ_{mtc} are omitted.) Conversely, when i is vacuum and j is occupied by a molecule, the molecule's move direction pd_i is replaced by $-pd_i$ in the above equation. Note that if the preferential directions are uniform over all of the sites, a free molecule without molecular interaction always maintains the directions of its TKEs after one full unit-time update, because whenever an inversion of TKE takes place, it is canceled by another inversion in the update scheme of Fig. 7. This does not hold, however, if the preferential directions are not uniform. This issue will be addressed again in section 3.6.

When both i and j are occupied by molecules, the two molecules exchange TKEs as in an elastic collision

$$\begin{aligned} mt_i \neq V \wedge mt_j \neq V \\ \Rightarrow \psi_{\text{mtc}}(tke_{i,\pm pd_i}, tke_{j,\pm pd_i}) = (tke_{j,\pm pd_i}, tke_{i,\pm pd_i}). \end{aligned} \quad (12)$$

3.4.2 Maintenance of molecular bonds

As mentioned earlier, polymers are composed as chains of monomers linked by molecular bonds (Fig. 5). Integrated and coherent motion of such a multi-site structure (“solid body”) is difficult to model using CA. A possible approach is to express the structure’s motion states by its deforming shape[24, 25]. Although this method can replicate many aspects of Hamiltonian mechanics as well as the structure’s integrity, it makes it difficult to formalize proper interaction between such a structure and the single-site particles (molecules) whose motion states are expressed as their internal states. In the RLMA, the maintenance of bonds is ensured by using the bond information as another conditional signal for the molecular translational permutation (11).

First, it is checked if the molecular bonds (provided they exist) are maintained when the molecule at i moves to the vacuum site $j = pd_i(i)$. Bonds with molecules at $\Delta^{\pm 1}(pd_i)(i)$ are not destroyed by the movement because the bonded molecules remain neighbors (the bond directions after movement become $\Delta^{\pm 2}(pd_i)$; Fig. 8(a)). If the molecule has bonds in other directions, these bonds are destroyed by the movement (Fig. 8(b)). Therefore, we append another condition to the permutation (11):

$$\begin{cases} mt_i \neq V, mt_j = V \Rightarrow \\ \text{Apply (11) followed by bond readjustment } \psi_{\text{br}} & \text{if } mb_{i,\Delta^{\pm 2}(pd_i)} = mb_{i,-pd_i} = 0, \\ \psi_{\text{mtc}}(\omega_i, \omega_j) = (\omega_i, \omega_j) & \text{otherwise.} \end{cases} \quad (13)$$

The readjustment of bonds ψ_{br} takes place not only at the moved molecule’s new position j but also at $\Delta^{\pm 1}(pd_i)(i)$ if the bonds exist:

$$\psi_{\text{br}} \begin{pmatrix} mb_{j,\Delta^+1(pd_i)}, mb_{j,\Delta^+2(pd_i)} \\ mb_{\Delta^+1(pd_i)(i),\Delta^-2(pd_i)}, mb_{\Delta^+1(pd_i)(i),\Delta^-1(pd_i)} \\ mb_{j,\Delta^-1(pd_i)}, mb_{j,\Delta^-2(pd_i)} \\ mb_{\Delta^-1(pd_i)(i),\Delta^+2(pd_i)}, mb_{\Delta^-1(pd_i)(i),\Delta^+1(pd_i)} \end{pmatrix} = \begin{pmatrix} 0, mb_{j,\Delta^+1(pd_i)} \\ 0, mb_{\Delta^+1(pd_i)(i),\Delta^-2(pd_i)} \\ 0, mb_{j,\Delta^-1(pd_i)} \\ 0, mb_{\Delta^-1(pd_i)(i),\Delta^+2(pd_i)} \end{pmatrix}, \quad (14)$$

A drawback of this rule is that it occasionally causes motion of polymers that has less physical relevance. For example, when a polymer’s constituent monomers are arranged on a straight line and all of the monomers have positive TKE only on the line, the polymer cannot move even if all of the monomers’ TKE directions are identical. However, if some of the monomers have positive TKEs in other directions, this polymer can move on average to its most proper direction with respect to TKE, while becoming deformed and keeping its integrity.

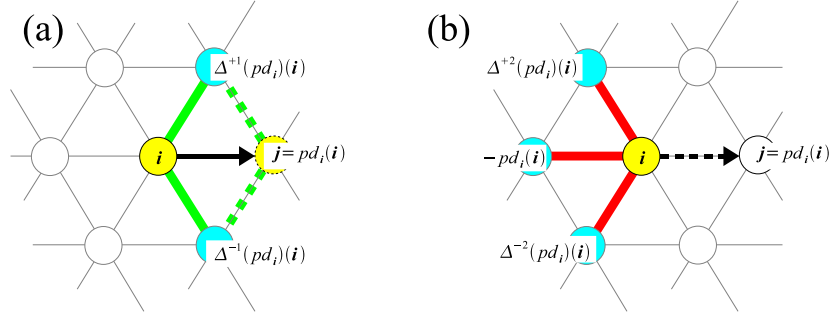


Figure 8: Translational movement and molecular bonds. If a molecule at i is moving to $j = pd_i(i)$, (a) its bonds in directions $\Delta^{\pm 1}(pd_i)$ are maintained with their directions readjusted to $\Delta^{\pm 2}(pd_i)$, but (b) bonds in directions $\Delta^{\pm 2}(pd_i)$ and $-pd_i$ would not be maintained.

3.4.3 Self-organization and reversibility

In irreversible models such as the LMA, the tendency of self-organization from disordered high-entropy states to ordered low-entropy structures is embedded in their information-losing transition rules themselves. To realize “apparent” self-organization of ordered structures by a reversible rule without information loss, the rule needs additional degrees of freedom that work as a *heat bath* into which the entropy generated in the organization process should be disposed of. The deterministic Ising model[8] and the reversible generalization[9] of the diffusion limited aggregation (DLA) model[26] are examples of this approach. We also adopt this approach, using the *heat particle layer* as the heat bath.

When both of the neighboring sites i and j have molecules, in advance of the collision (12) by ψ_{mtc} , we apply site-respective TKE–heat interaction ψ_{th} defined as follows. For the molecule at site x (i.e., either i or j), when it has positive TKE in one direction l out of $\{\pm pd_i\}$ (i.e., along the line connecting the two molecules), and when the heat particles satisfy $h_{x,l} < H_{max}$ and $h_{x,-l} = 0$ at site x , then the positive TKE is transformed into a heat particle in the same direction l (heat release):

$$\begin{cases}
 mt_i \neq V, mt_j \neq V \text{ then for } x \in \{i, j\} \\
 \psi_{th} \begin{pmatrix} tke_{x, \pm pd_i} \\ h_{x, \pm pd_i} \end{pmatrix} = \begin{pmatrix} tke_{x, \pm pd_i} - 1 \\ h_{x, \pm pd_i} + 1 \end{pmatrix} & \text{if } (tke_{x, \pm pd_i}, tke_{x, \mp pd_i}) = (1, 0) \\
 & \text{and } h_{x, \pm pd_i} < H_{max}, h_{x, \mp pd_i} = 0, \\
 \psi_{th}(\omega_x) = \omega_x & \text{otherwise.}
 \end{cases} \quad (15)$$

On the other hand, when the molecule at x does not have a TKE in either of $\{\pm pd_i\}$ and heat particles exist in only one of the two directions, one heat

particle is transformed into the TKE in the same direction (heat absorption):

$$\left\{ \begin{array}{l} mt_i \neq V, mt_j \neq V \text{ then for } \mathbf{x} \in \{\mathbf{i}, \mathbf{j}\} \\ \psi_{\text{th}} \left(\begin{array}{c} tke_{\mathbf{x}, \pm pd_i} \\ h_{\mathbf{x}, \pm pd_i} \end{array} \right) = \left(\begin{array}{c} tke_{\mathbf{x}, \pm pd_i} + 1 \\ h_{\mathbf{x}, \pm pd_i} - 1 \end{array} \right) \quad \begin{array}{l} \text{if } (tke_{\mathbf{x}, pd_i}, tke_{\mathbf{x}, -pd_i}) = (0, 0) \\ \text{and } h_{\mathbf{x}, \pm pd_i} > 0, h_{\mathbf{x}, \mp pd_i} = 0, \\ \text{otherwise.} \end{array} \\ \psi_{\text{th}}(\omega_{\mathbf{x}}) = \omega_{\mathbf{x}} \end{array} \right. \quad (16)$$

Introduction of this TKE–heat interaction makes the interaction between neighboring molecules non-elastic.

For molecular translation, potentials work as yet another control signal for the permutation in ψ_{mtc} of Eq. (11), and the translation is executed only if the changes in potentials entailed by the movement of molecule from \mathbf{i} to \mathbf{j} , given that their neighbors are fixed, can be compensated for by emission/absorption of heat particles at \mathbf{i} and \mathbf{j} :

$$\left\{ \begin{array}{l} mt_i \neq V, mt_j = V \Rightarrow \\ \text{Proceed to (13)} \quad \begin{array}{l} \text{if } 0 \leq h_{i,l} - \delta^{(-)}V^{i,l(i)} \leq H_{\text{max}} \text{ and} \\ 0 \leq h_{j,l} - \delta^{(+)}V^{j,l(j)} \leq H_{\text{max}} \text{ for } l \in L, \\ \text{otherwise.} \end{array} \\ \psi_{\text{mtc}}(\omega_i, \omega_j) = (\omega_i, \omega_j) \end{array} \right. \quad (17)$$

Here, $\delta^{(-)}V^{i,l(i)}$ represents the potential change in direction l caused by removing the molecule from its current site \mathbf{i} , and $\delta^{(+)}V^{j,l(j)}$ represents a potential change in direction l caused by placing the molecule (while maintaining its orientation) at vacuum site \mathbf{j} . Further, when the translation is actually induced by the permutation (11), it is followed by the potential change compensation ψ_{pcc} :

$$\psi_{\text{pcc}}((h_{i,l})_l, (h_{j,l})_l) = \left((h_{i,l} - \delta^{(-)}V^{i,l(i)})_l, (h_{j,l} - \delta^{(+)}V^{j,l(j)})_l \right). \quad (18)$$

Thus, a molecule moving to a more stable site ($\sum_l \delta^{(+)}V^{j,l(j)} < 0$) releases heat particles in total, and it can be dissociated again from its neighbors only when enough energy is supplied by the heat particle layer.

3.4.4 Rotation of polar molecules

Polar molecules such as water and hydrophilic monomers can take different potential values depending on their orientations. According to the LMA rule, the polar molecules are rotated irreversibly into their more stable (lower-potential) orientations. To maintain reversibility and at the same time to enable relaxation into a more stable direction configuration, we utilize RKE and also the heat particle layer. Similar to the paired site interaction in Fig. 7, rotational update is also performed in the interleaved scheme shown in Fig. 9. Here, we again use the site groups of Eq. (9) (although for the rotational permutation given below, interference can be prevented if the sites in each group are separated by more than a unit distance).

```

start
for  $g$  in site groups  $G$  do
  for every  $i$  in a group  $g$  do
    if  $mt_i \in \{W, I\}$  then //polar molecule
       $\rho(mo_i, rke_i, (h_{i,l})_{l \in L});$  //rotational update
    end
  end

```

Figure 9: Interleaved update scheme for molecular orientation and RKE with heat interaction.

The rotational update ρ is defined as follows: the polar molecule at i rotates according to the sign of RKE and the orientation becomes $\Delta^{rke_i}(mo_i)$ if the change in potentials caused by the rotation can be compensated for by emission/absorption of heat particles at the site. Otherwise, the molecule does not rotate and RKE is inverted:

$$\rho \begin{pmatrix} mo_i \\ rke_i \\ (h_{i,l})_l \end{pmatrix} = \begin{cases} \begin{pmatrix} \Delta^{rke_i}(mo_i) \\ rke_i \\ (h_{i,l} - \delta(mo_i, \Delta^{rke_i})V^{i,l(i)})_l \end{pmatrix} \\ \text{if } 0 \leq h_{i,l} - \delta(mo_i, \Delta^{rke_i})V^{i,l(i)} \leq H_{\max} \text{ for } \forall l \in L, \\ \begin{pmatrix} mo_i \\ -rke_i \\ (h_{i,l})_l \end{pmatrix} & \text{otherwise.} \end{cases} \quad (19)$$

Here

$$\delta(k, \Delta^n)V^{i,l(i)} \quad (20)$$

represents the potential change in direction l that occurs when the orientation of the molecule at i is changed from k to $\Delta^n(k)$, with the neighboring molecules fixed.

In this rule, the RKEs work as a kind of “second-order” signal[10], which preserves the history of the molecules’ rotational states. Therefore, the polar molecules cannot stop rotating i.e., $rke \neq 0$ (or given $rke \neq 0$ as the initial condition, they cannot change their orientations forever). For an alternative rotation rule that allows RKEs to take values on \mathbb{Z} , including the stationary state $rke = 0$, see Appendix A.

3.4.5 Transportation of heat particles

For the heat particle layer to function as a heat bath, the released heat particles should be effectively diffused into open areas. In our RLMA model, the diffusion of heat particles is conducted by a rule similar to that for the Frisch–Hasslacher–Pomeau lattice gas automata (FHP-LGA)[13], that is, for every unit-time update, a synchronous shift (translation) σ_h is performed in each direction

$$\sigma_h : h_{i,l} \mapsto h_{-l(i),l} \quad \text{for } l \in L \quad (21)$$

followed by a local collision ϕ_h at each site:

$$\phi_h : \begin{cases} ((h_{i,\Delta^l(k)})) = (m, 0, 0, m, 0, 0) & \mapsto \begin{cases} (0, m, 0, 0, m, 0) & \text{if parity}(pd_i) = +1, \\ (0, 0, m, 0, 0, m) & \text{if parity}(pd_i) = -1, \end{cases} \\ ((h_{i,\Delta^l(k)})) = (m, 0, m, 0, m, 0) & \mapsto (0, m, 0, m, 0, m) \\ ((h_{i,\Delta^l(k)})) & \mapsto ((h_{i,\Delta^l(k)})) \quad \text{otherwise} \end{cases} \quad (22)$$

with $0 < m \leq H_{\max}$ and $k \in \{1, 2, 3\}$. Note that the collision ϕ_h is deterministic and utilizes the parity of preferential direction at each site.

3.5 Composition of unit-time update

After integrating the sub-steps defined above, a unit-time update of the RLMA can be performed through the following time sub-steps (variables in parentheses are those affected by the particular sub-step):

1. Transportation of heat particles $((h_{i,l}), pd_i)$
Heat particles are diffused by the FHP-LGA-like combination of the shift (21) and collision (22).
2. Rotation of polar molecules $(mt_i, mo_i, rke_i, (h_{i,l}))$
Using the interleaved scheme of Fig. 9, molecular rotation is performed by the conditional permutation (19).
3. Molecular translation and interaction $(mt_i, mo_i, (tke_{i,l}), (mb_{i,l}), (h_{i,l}), pd_i)$
Using the interleaved scheme of Fig. 7,
 - molecular translation is performed by the paired site conditional permutation (11) with the conditions (13) and (17), while
 - molecular interaction is performed by the conditional permutation (12) with the heat release (15) and absorption (16).
4. Update of preferential direction (pd_i)
To ensure unbiasedness for the principal directions, the preferential direction should be updated according to time. We use the simple uniform rotation $pd_i \mapsto \Delta^{+1}(pd_i)$, although synchronous shifts and deterministic, invertible pseudorandom number generators can also be combined.

These sub-steps are independent; therefore, the order can be changed. Each sub-time step is reversible; therefore, the inverse update is achieved by performing this construction in reverse.

3.6 Conservation laws

From the above definitions, the transition rule of RLMA conserves *mass* (number of molecules) and the *total energy* that is given as a sum of TKEs, RKEs,

potential energies, and heat particles over the sites:

$$E_{\text{total}} = \sum_i \sum_{l \in L} tke_{i,l} + \sum_i |rke_i| + V_{\text{total}} + \sum_i \sum_{l \in L} h_{i,l}. \quad (23)$$

These conservation laws enable precise application and validation of methods and theorems in statistical mechanics, both equilibrium (microcanonical, canonical, and grand-canonical) and nonequilibrium (*e.g.*, relaxation, Fourier’s law of heat conduction, Green–Kubo relations), as is done for simpler (and in many cases more abstract) CA models[8, 9, 27, 28, 29, 30, 31, 32].

On the other hand, conservation of momenta does not hold because of the TKE inversion in the translational permutation (11), as mentioned in section 3.4.1. (Angular momenta are not conserved either, because the rotational permutation (19) also contains uncompensated inversion of RKE.) From the macroscopic viewpoint, this non-conservation of momenta seems to work positively to enhance the model’s ergodicity, instead of the effect of chaos dynamics, which discrete CA models lack.

4 Simulation

In this section, we demonstrate by simulation that the RLMA can reproduce the original LMA’s self-organization results[3] as special cases. We also show that the RLMA reproduces results which are qualitatively consistent with the traditional Larson-type models. More extensive results and their statistical treatment will be given in a future work.

In the following simulations, the parameters are set as follows: $H_{\text{max}} = 8$, $V_{\text{WH-WH}} = V_{\text{WO-WO}} = V_{\text{WO-IP}} = V_{\text{IP-IP}} = +4$, $V_{\text{WH-WO}} = V_{\text{WH-IP}} = -4$, $V_{\text{WH-WN}} = V_{\text{WH-IN}} = V_{\text{WH-O}} = V_{\text{WO-WN}} = V_{\text{WO-IN}} = V_{\text{WO-O}} = V_{\text{IP-WN}} = V_{\text{IP-IN}} = V_{\text{IP-O}} = V_{\text{O-O}} = -1$. The simulations in section 4.1 and 4.2 adopted lattice space consisting of $N = 24 \times 24$ cells, while the simulations in section 4.3 used lattice space of $N = 100 \times 100$ cells. Periodic boundary condition is applied in all the simulations, so the systems are isolated.

4.1 Hydrophobic monomers in a polar environment

Fig. 10 shows snapshots of the molecular layer in a simulation of a mixture of water and hydrophobic monomers (25% water, 25% hydrophobic monomer, 50% vacuum). Starting from a homogeneously mixed initial configuration with no heat particles (Fig. 10(a)), clustering and phase separation gradually take place (Fig. 10(b), (c)), accompanied by emission of heat particles (not shown in the figures).

Note also that phase separation takes place in spite of the setup that the induction-based forces $v_{\text{WO-H}}$ and $v_{\text{WO-O}}$ between a hydrophobic monomer and a water molecule are set equal to the dispersion interaction force v_{OO} between two hydrophobic monomers, and they are much weaker than the water–water

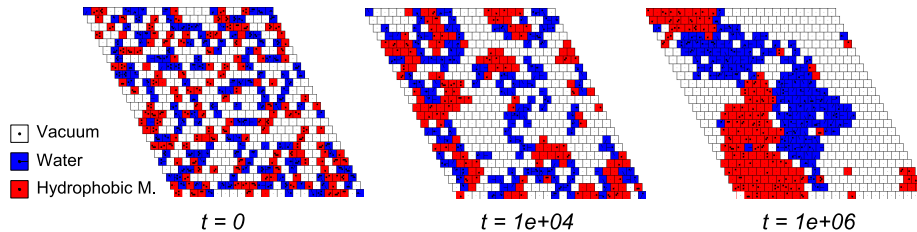


Figure 10: Snapshots of the molecular layer in a simulation of a water–hydrophobic monomer system. The molecules cluster preferentially with those of the same type, and phase separation occurs.

binding $v_{\text{WH-VO}}$, as is the case in Ref. [3] (see also section 2.3). Since the system is isolated, this self-organization process is *entropy-driven*.

Fig. 11 shows the time evolution of mean energies per cell—TKE (sum for all of the principal directions $\langle \sum_{l \in L} tke_{i,l} \rangle_i$), RKE (absolute value $\langle |rke_i| \rangle_i$), potential energy (sum for all of the principal directions $\frac{1}{2} \langle \sum_{l \in L} V^{i,l} \rangle_i$), heat particles (sum for all of the principal directions $\langle \sum_{l \in L} h_{i,l} \rangle_i$)—in the simulation run of Fig. 10. In this relaxation process, as the molecules are organized into

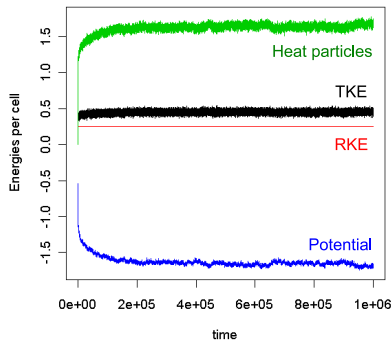


Figure 11: Time evolution of mean values of TKE, RKE, potential energy, and heat particles per cell in a simulation of a water–hydrophobic monomer system.

a more stable configuration, the energy released from the molecular layer is transferred into the heat particle layer, with the total energy conserved (mean total energy per cell, $e_{\text{total}} = E_{\text{total}}/N$, is 0.68). It is observed that a large part of the energy transfer takes place in the first few thousand steps. This corresponds to quick dissolution of high-potential, unstable partial configurations.

Fig. 12 shows the time evolution of mean numbers of neighboring molecules

of the same types (water and hydrophobic monomer)—calculated as $\langle |\{l(i) | mt_{l(i)} = X\}| \rangle_{i \text{ s.t. } mt_i = X}$ for $X = W, O$, respectively—in the same simulation. The mean neighboring molecules of the same types start from the initial random

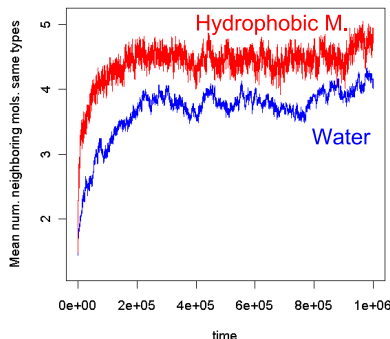


Figure 12: Time evolution of mean numbers of neighboring molecules of the same types (water and hydrophobic monomer) in the simulation of a water–hydrophobic monomer system.

configuration (where the value $\sim 0.25 \times 6 = 1.5$ for both water and hydrophobic monomers) and increase relatively slowly, taking a few million steps to reach the equilibrium state. This result is consistent with observations of the physico-chemical molecular aggregation process, where small clusters are quickly formed, but as the size grows, their mobility decreases and integration into larger clusters requires more time.

4.2 Amphiphilic polymers in a polar environment

Fig. 13 shows snapshots of the molecular layer in three simulations of amphiphilic tetramers (each consisting of three hydrophilic monomers plus one hydrophobic head monomer, see Fig. 5) in solvent water, with different settings for the initial distribution of heat particles.

In the simulation of Fig. 13(a), initially, there are no heat particles, representing the “low-temperature” condition (mean total energy per cell $e_{\text{total}} = 0.95$). Although the low-temperature condition is the same as the one adopted in the simulation of Fig. 10, this simulation requires a longer relaxation time, because the polymers’ mobility is lower than that of the monomers (mainly because of the bond maintenance condition (13)). Starting from the initial condition where the tetramers are homogeneously distributed, they aggregate into micelle-like structures, their hydrophilic heads staying in contact with water and their hydrophobic tails trying to cluster. The micelle-like structures are an elementary example of *higher-order* structures[1], with emergent properties such as integrity

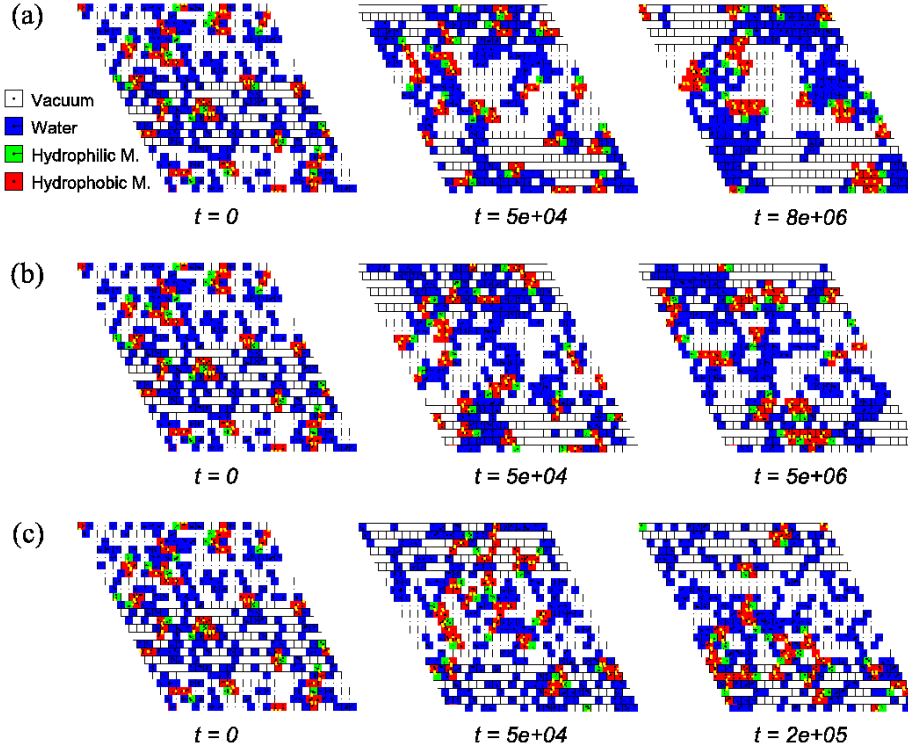


Figure 13: Snapshots of the molecular layer in three simulations of water-amphiphilic polymer systems with different initial distributions of heat particles (“temperature”): (a) low-, (b) moderate-, and (c) high-temperature conditions.

and even lower mobility.

Fig. 13(b) corresponds to the “moderate-temperature” condition, where the initial $h_{i,l}$ is given randomly from $[0, 1]$ with $\langle h_{i,l} \rangle_i = 1$ for $l \in L$ (mean total energy per cell $e_{\text{total}} = 3.93$). Compared with the low-temperature condition, while the sizes of the organized micelle-like structures and water aggregates become smaller, their motion becomes faster.

Fig. 13(c) corresponds to the “high-temperature” condition, where the initial $h_{i,l}$ is given randomly from $[0, 4]$ with $\langle h_{i,l} \rangle_i = 2$ for $l \in L$ (mean total energy per cell $e_{\text{total}} = 13.01$). In this condition, the molecular motion becomes even faster and no distinct self-organization is observed.

Fig. 14 shows the time evolution of mean energies per cell, and Fig. 15 shows the time evolution of mean numbers of neighboring molecules of the same types (water and hydrophobic monomer) in the three abovementioned simulations with the different temperature conditions. Note the difference in the time scales. These results indicate the temperature dependency of the molecular pro-

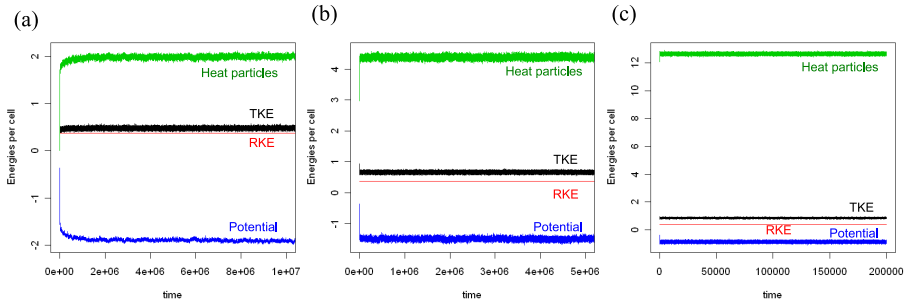


Figure 14: Time evolution of mean values of TKE, RKE, potential energy, and heat particles per cell in a simulation of water-amphiphilic polymer systems in the different temperature conditions: (a) low-, (b) moderate-, and (c) high-temperature conditions.

cess. That is, at lower temperature, polymers aggregate into larger structures; however, the formation process takes a longer time. On the other hand, at higher temperature, large structures cannot be maintained while the motion of polymers gets faster. This kind of temperature dependency is derived (rather than being presupposed) in a precise manner only from dynamical models with reversibility and energy conservation. Fig. 15 (especially (a)) also shows that the aggregation of polymers is slower than the clustering of water.

4.3 Phase separation dynamics in ternary mixtures

To compare in more detail the behavior of our RLMA with experimental observations and other models (especially the Larson-type ones), we conducted simulation of ternary mixtures of water, hydrophobic monomers, and amphiphilic polymers, and analyzed the phase separation dynamics with different concentration and temperature (total energy) settings.

Theories as well as successful models have shown that the phase separation or domain growth dynamics generally obeys dynamic scaling[33, 15, 34, 36, 22], where domain structure remains statistically invariant in time under rescaling by the characteristic length scale L , and L grows as a function of time following the asymptotic power law, $L(t) \sim t^{1/z}$. The theories typically suggest $z = 1/3$, though the value can differ depending on the stages of phase separation.

To check if the RLMA realizes the dynamic scaling behavior, we investigated the evolution of *mean cluster radius*. A molecule of type X (in this case, X can be water W, hydrophobic monomer O, or amphiphile A) belongs to a cluster of type X if any of its nearest neighbor are of the same type and are already counted as part of the cluster. Using the cluster distribution $\{n_X(s)\}_s$, where $n_X(s)$ is the number of type X clusters with size s , the mean cluster size χ_X of

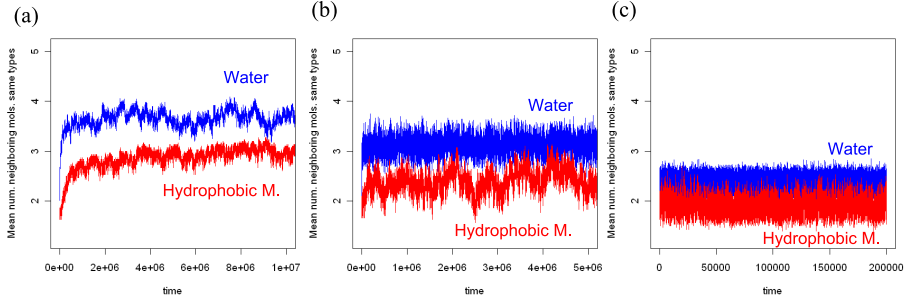


Figure 15: Time evolution of mean numbers of neighboring molecules of the same types (water and hydrophobic monomer) in the simulations of water–amphiphilic polymer systems with the different temperature conditions: (a) low-, (b) moderate-, and (c) high-temperature conditions.

type X is estimated as

$$\chi_X = \frac{\sum_{s=1}^{s_{\max,X}-1} s^2 n_X(s)}{\sum_{s=1}^{s_{\max,X}} s n_X(s)}, \quad (24)$$

where $s_{\max,X}$ is the largest cluster of type X . In two dimensions, the mean cluster radius of type X is estimated as $R_X \sim \chi_X^{1/2}$.

Fig. 16 shows the evolution of averaged mean cluster radius $\langle R \rangle = [\frac{1}{2}(\chi_W + \chi_O)]^{1/2}$, with different concentration ratios of water ϕ_W , hydrophobic monomers ϕ_O , and amphiphilic polymers ϕ_A (the ratio of vacuum $\phi_V = 0.4$ is common), in a temperature setting (mean total energy $e_{\text{total}} = 1.18$). Power law behavior is observed for all the concentration ratios $(\phi_W, \phi_O, \phi_A) = (0.288, 0.288, 0.024)$, $(0.27, 0.27, 0.06)$, and $(0.24, 0.24, 0.12)$. For each setting, the scaling exponent $1/z$ is estimated as 0.213 ± 0.004 , 0.199 ± 0.005 , and 0.121 ± 0.004 , by fitting the data within time region $[10000, 200000]$ into $\langle R \rangle(t) \sim t^{1/z}$. These estimated values, especially the former two ($1/z \sim 0.2$) are similar to the ones obtained by simpler Ising spin models for binary systems [34, 35, 36], but smaller than the theoretical value $z = 1/3$ which is also obtained in Ref. [22] by adding small amount of amphiphile into binary mixture, like in this simulation. The small values are possibly because the asymptotic late stage is not reached due to the small size of the system, but other possible reasons can be also suggested: (i) the existence of hydrodynamics, which is supposed to be absent in the dynamic scaling hypothesis[33] as well as the Larson-type model in Ref. [22], (ii) the constant-energy condition, where the temperature increases as the clustering proceeds and the dynamic exponent becomes smaller compared to the isothermal condition[15], while the latter is usually used in the Larson-type models and other Monte Carlo methods, and (iii) other conservation laws, which also work to decrease the exponent [36]. The decrease in the growth rate of $\langle R \rangle$

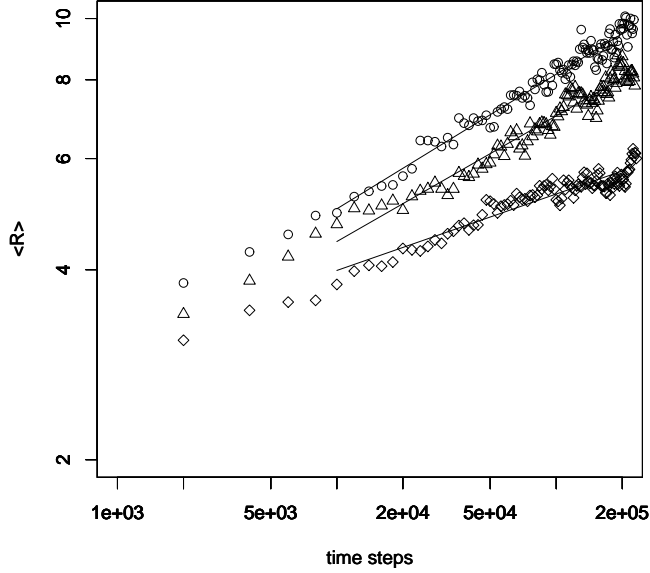


Figure 16: Time evolution of the averaged mean cluster radius $\langle R \rangle$, with different molecular ratios. \circ represents $(\phi_W, \phi_O, \phi_A) = (0.288, 0.288, 0.024)$, \triangle represents $(\phi_W, \phi_O, \phi_A) = (0.27, 0.27, 0.06)$, and \diamond represents $(\phi_W, \phi_O, \phi_A) = (0.24, 0.24, 0.12)$. The lines show power law relations with estimated scaling exponents $1/z$ for their slopes.

accompanying the increase of concentration ϕ_A of amphiphile is consistent with the result in Ref. [22].

For different temperature settings we also calculated the *equal-time structure factors* $S_X(k, t)$, which is the Fourier transform of the *equal-time pair correlation function*, defined as

$$S_X(k, t) = \int C_{XX}(\vec{r}, t) e^{i\vec{k} \cdot \vec{r}} d\vec{r}, \quad (25)$$

$$C_{XX}(\vec{r}, t) = \langle \delta\rho_X(\vec{r}, t) \delta\rho_X(\vec{0}, t) \rangle. \quad (26)$$

The equal-time pair correlation $C_{XX}(\vec{r}, t)$ of type X is calculated by drawing shells of radius r and $r + 1$ around each molecule of type X , counting the number of the same type molecules between the shells, and finally normalizing by dividing by r .

Fig. 17 shows the equal-time water–water structure factor $S_W(k, t)$ for a system with $(\phi_W, \phi_O, \phi_A) = (0.288, 0.288, 0.024)$ and different temperature (total energy) settings. In the lower temperature settings as Fig. 17(a) and (b) (mean

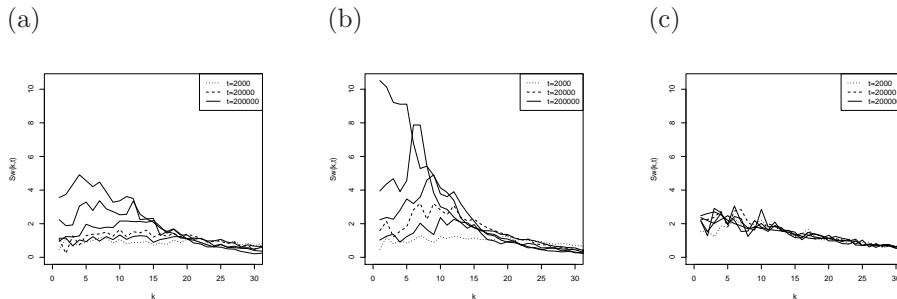


Figure 17: The equal-time water–water structure factor for a system with $(\phi_W, \phi_O, \phi_A) = (0.288, 0.288, 0.024)$ and different temperature (total energy) settings: (a) $e_{\text{total}} = 0.37$, (b) $e_{\text{total}} = 1.18$, (c) $e_{\text{total}} = 5.63$. $S_W(k, t)$ at times $t = 2, 10, 20, 50, 100, 200 \times 10^3$ are shown.

total energy $e_{\text{total}} = 0.37$ and $e_{\text{total}} = 1.18$, respectively), the structure factor develops a peak at nonzero wave number that grows in time and the position of the peak moves to lower k as t increases. The peak at $k \sim 1$ indicates that the system is approaching to a global separation into spanning networks. The growth rate of the peak is higher for the “warm” condition $e_{\text{total}} = 1.18$ than the “cool” condition $e_{\text{total}} = 0.37$. Above a critical total energy (that corresponds to the *demixing temperature*), as Fig. 17(c) ($e_{\text{total}} = 5.63$), the structure factor does not show any structure. These are again in good agreement with the result in Ref. [22], as well as experiment[37].

5 Conclusion

In this paper, we described the construction of RLMA, which simulates physico-chemical interaction of molecules and their self-organization process. The definition of the model has shown how to eliminate the irreversibility in the original LMA using several techniques to construct reversible CA. Simulation results of RLMA dynamics have demonstrated that the RLMA can deal with broader situations, with the original LMA’s self-organization results as special cases. The results also showed that the RLMA reproduces qualitatively consistent results with the traditional Larson-type models.

Although several reversible CA models have been proposed to simulate self-organization processes[8, 9], to our knowledge, this is the first deterministic CA model that simulates self-organization of *higher-order* structures, while satisfying strict reversibility.

Reversibility and conservation laws of the model enable precise application and validation of the various methods in both equilibrium and nonequilibrium statistical mechanics. Reversibility also enables rigorous tracking of the information flow driven by the dynamics, with no veiled sources or sinks. Therefore,

the model will be preferable in analyzing the self-organization and dynamics of multiple levels of structures from an information-theoretic viewpoint (*e.g.*, Ref. [2]), as well as from the physically grounded viewpoint.

This study focused on the process of molecular assembly. However, the model can be extended to incorporate chemical reactions and catalytic effects, by introducing more types of molecules and setting proper values of excitation energies for the reactions, with their modulation in the existence of neighboring catalytic molecules. We are currently working on the construction of such a reversible and thermodynamically consistent model that realizes “protocells” [6] with self-maintenance of compartment structures, metabolism, and self-reproduction.

Acknowledgments

This study was in part supported by “Symbiotic Information Technology Research Project” of Tokyo University of Agriculture and Technology, and also by the Grant-in-Aid for “Scientific Research on Priority Areas (Area No. 454)” from the Japanese Ministry of Education, Culture, Sports, Science and Technology.

A Alternative implementation of molecular rotation

Here, we present an alternative rotation rule, which enables the stationary state $rke = 0$ for the polar molecules. Using the same interleaved scheme of Fig. 9, the rotational permutation ρ of (19) is replaced by the new conditional permutation ρ_a defined below.

First, consider that a polar molecule at \mathbf{i} is rotating, *i.e.*, $rke_{\mathbf{i}} \neq 0$. Then, ρ_a maintains the rotation and changes the molecule’s orientation by $\Delta^{\text{sgn}(rke_{\mathbf{i}})}$ ³ if the magnitude of $rke_{\mathbf{i}}$ is more than sufficient to compensate for the change in potential induced by the rotation; else, it inverts the direction of rotation if the magnitude of $rke_{\mathbf{i}}$ is not large enough. If the magnitude of $rke_{\mathbf{i}}$ is just sufficient to compensate for the potential change, ρ_a either executes the rotation and brings the molecule to the stationary state, or inverts the direction of rotation,

³The sign function, $\text{sgn}(rke_{\mathbf{i}}) = +1$ if $rke_{\mathbf{i}} > 0$, -1 if $rke_{\mathbf{i}} < 0$, indicates the direction of rotation.

depending on some conditions to avoid irreversibility:

$$\rho_a \begin{pmatrix} mo_i \\ rke_i \end{pmatrix} = \left\{ \begin{array}{l} \begin{pmatrix} \Delta^{\text{sgn}(rke_i)}(mo_i) \\ rke_i - \text{sgn}(rke_i)\delta(mo_i, \Delta^{\text{sgn}(rke_i)})V^i \end{pmatrix} \quad \text{if } rke_i \neq 0 \text{ and} \\ \left\{ \begin{array}{l} |rke_i| > \delta(mo_i, \Delta^{\text{sgn}(rke_i)})V^i, \text{ or} \\ |rke_i| = \delta(mo_i, \Delta^{\text{sgn}(rke_i)})V^i \\ \wedge \delta(\Delta^{\text{sgn}(rke_i)}(mo_i), \Delta^{\text{sgn}(rke_i)})V^i \geq 0, \text{ or} \\ |rke_i| = \delta(mo_i, \Delta^{\text{sgn}(rke_i)})V^i \\ \wedge \delta(\Delta^{\text{sgn}(rke_i)}(mo_i), \Delta^{\text{sgn}(rke_i)})V^i < 0 \\ \wedge \text{parity}(pd_i) \neq \text{sgn}(rke_i), \end{array} \right\} \\ \begin{pmatrix} mo_i \\ -rke_i \end{pmatrix} \quad \text{if } rke_i \neq 0 \text{ and} \\ \left\{ \begin{array}{l} |rke_i| < \delta(mo_i, \Delta^{\text{sgn}(rke_i)})V^i, \text{ or} \\ |rke_i| = \delta(mo_i, \Delta^{\text{sgn}(rke_i)})V^i \\ \wedge \delta(\Delta^{\text{sgn}(rke_i)}(mo_i), \Delta^{\text{sgn}(rke_i)})V^i < 0 \\ \wedge \text{parity}(pd_i) = \text{sgn}(rke_i). \end{array} \right\} \end{array} \right. \quad (27)$$

Next, consider that a polar molecule at i is in the stationary state, i.e., $rke_i = 0$. Then, ρ_a starts the rotation if changing the molecule's orientation by one of the directions $\Delta^{\pm 1}$ induces a negative potential change. If rotations in both of the directions $\Delta^{\pm 1}$ induce negative potential changes, ρ_a starts the rotation according to the preferential direction. On the other hand, if the molecule's orientation is at a local potential minimum, the molecule maintains its stationary state:

$$\rho_a \begin{pmatrix} mo_i \\ rke_i \end{pmatrix} = \left\{ \begin{array}{l} \begin{pmatrix} \Delta^{\pm 1}(mo_i) \\ \mp \delta(mo_i, \Delta^{\pm 1})V^i \end{pmatrix} \quad \text{if } rke_i = 0 \text{ and} \\ \left\{ \begin{array}{l} \delta(mo_i, \Delta^{\pm 1})V^i < 0 \\ \wedge \delta(mo_i, \Delta^{\mp 1})V^i \geq 0, \text{ or} \\ \delta(mo_i, \Delta^{\pm 1})V^i < 0 \\ \wedge \delta(mo_i, \Delta^{-1})V^i < 0 \wedge \text{parity}(pd_i) = \pm 1, \end{array} \right\} \\ \begin{pmatrix} mo_i \\ 0 \end{pmatrix} \quad \text{if } rke_i = 0 \text{ and} \\ \delta(mo_i, \Delta^{+1})V^i \geq 0 \wedge \delta(mo_i, \Delta^{-1})V^i \geq 0. \end{array} \right. \quad (28)$$

Here

$$\delta(k, \Delta^n)V^i = \sum_{l \in L} \delta(k, \Delta^n)V^{i,l(i)} \quad (29)$$

represents the total potential change at i that occurs when the orientation of the molecule at i is changed from k to $\Delta^n(k)$ (see the notation (20), too).

The main point is that, in ρ_a , change in RKE and not heat compensates for the change in potential. Therefore, the RKE layer can work as another energy storage. Recall that in the rotation rule (19), RKE works just as ‘‘second-order’’ signals to preserve reversibility; hence, it cannot change to 0. It should also be noted that the parity (7) of the preferential direction is utilized to avoid non-

uniqueness of the ρ_a 's pre-images, which could be derived from unstable fixed points (stationary states at orientations of local maximum potential).

One drawback of this alternative rotation rule is that the value of RKE is unbounded in principle; thus, the model is not a CA in the strict sense. In practice, however, due to the energy conservation (23), limitless divergence of RKE cannot occur unless an infinite amount of energy is injected into a finite region.

The RLMA model with the alternative rotation permutation ρ_a shows qualitatively similar behavior. Fig. 18 shows snapshots of the molecular layer, Fig. 19 shows the time evolution of mean energies per cell, and Fig. 20 shows the time evolution of mean numbers of neighboring molecules of the same types in a simulation of a water–hydrophobic monomer system, with the same initial configuration as that in section 4.1.

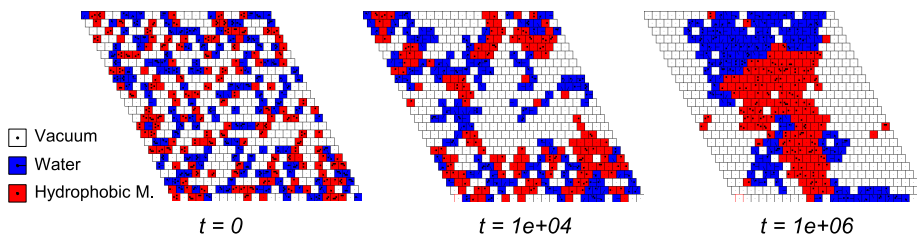


Figure 18: Snapshots of the molecular layer in a simulation of a water–hydrophobic monomer system, using the alternative rotation rule ρ_a . Clustering and phase separation occur in a similar manner to those shown in Fig. 10.

References

- [1] S. Rasmussen, N. A. Baas, B. M. M. Nilsson, and M. W. Olesen, *Artif. Life* **7**, 329 (2001).
- [2] S. McGregor and C. Fernando, *Artif. Life* **11**, 459 (2005).
- [3] B. Mayer, G. Köhler, and S. Rasmussen, *Phys. Rev. E* **55**, 4489 (1997).
- [4] B. Mayer and S. Rasmussen, *Int. J. Mod. Phys. C* **9**, 157 (1998).
- [5] B. Mayer and S. Rasmussen, *Int. J. Mod. Phys. C* **11**, 809 (2000).
- [6] N. Ono, *BioSystems* **81**, 223 (2005).
- [7] T. J. Hutton, *Artif. Life* **13**, 11 (2007).
- [8] M. Creutz, *Annals of Physics* **167**, 62 (1986).
- [9] R. M. D’Souza, *Phys. Rev. E* **60**, 264 (1999).

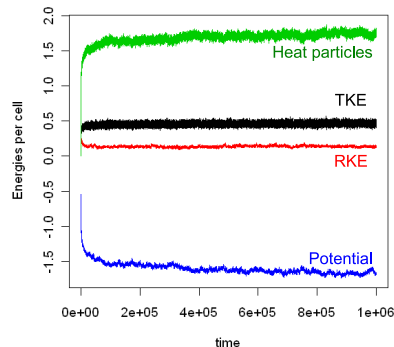


Figure 19: Time evolution of mean values of energies per cell in a simulation of a water–hydrophobic monomer system, using ρ_a . The mean absolute value of RKE $\langle|rke_i| \rangle_i$ fluctuates; this is in contrast to Fig. 11 where the value is constant.

- [10] T. Toffoli and N. Margolus, *Physica D* **45**, 229 (1990).
- [11] T. Toffoli, S. Capobianco, and P. Mentrasti, *Theor. Comput. Sci.* **325**, 329 (2004).
- [12] J. Hardy, Y. Pomeau, and O. de Pazzis, *J. Math. Phys.* **14**, 1746 (1973).
- [13] U. Frisch, B. Hasslacher, and Y. Pomeau, *Phys. Rev. Lett.* **56**, 1505 (1986).
- [14] K. Morita and M. Harao, *Trans. IEICE Japan* **E72**, 758 (1989).
- [15] S. W. Koch, R. C. Desai, and F. F. Abraham, *Phys. Rev. A* **27**, 2152 (1983).
- [16] R. G. Larson, L. E. Scriven, and H. T. Davis, *J. Chem. Phys.* **83**, 2411, (1985).
- [17] R. G. Larson, *J. Chem. Phys.* **89**, 1642, (1988).
- [18] R. G. Larson, *J. Chem. Phys.* **91**, 2479, (1989).
- [19] D. Stauffer, N. Jan and R. B. Pandey, *Physica A* **198** 401 (1993).
- [20] M. Sahimi and P. Nowrozi, *Phys. Rev. Lett.* **73** 1182 (1994).
- [21] T. B. Liverpool and A. T. Bernardes, *J. Phys. (France) II* **5** 1457 (1995).
- [22] A. T. Bernardes and T. B. Liverpool and D. Stauffer, *Phys. Rev. E* **54** R2220 (1996).

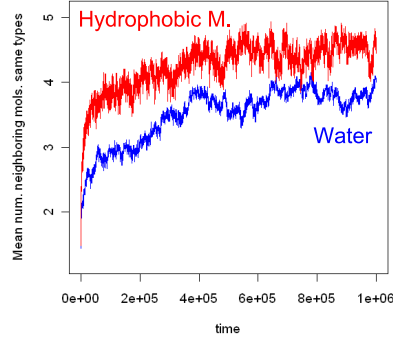


Figure 20: Time evolution of mean numbers of neighboring molecules of the same types in the simulation of a water–hydrophobic monomer system, using ρ_a . The evolution is similar to that shown in Fig. 12.

- [23] P. L. Privalov and S. J. Gill, *Pure Appl. Chem.* **61**, 1097 (1989).
- [24] B. Chopard, *J. Phys. A: Math. Gen.* **23**, 1671 (1990).
- [25] S. Marconi, Ph.D. thesis, UNIVERSITÉ DE GENÈVE, 2003.
- [26] J. T. A. Witten and L. M. Sander, *Phys. Rev. Lett.* **47**, 1400 (1981).
- [27] S. Takesue, *Physica D* **45**, 278 (1990).
- [28] S. Takesue, *Phys. Rev. Lett.* **64**, 252 (1990).
- [29] S. Takesue, *Physica D* **103**, 190 (1997).
- [30] T. Niwa, *J. Stat. Phys.* **89**, 801 (1997).
- [31] K. Saito, S. Takesue, and S. Miyashita, *Phys. Rev. E* **59**, 2783 (1999).
- [32] D. Stauffer, *Comput. Phys. Commun.* **127**, 113 (2000).
- [33] K. Binder and D. Stauffer, *Phys. Rev. Lett.* **33**, 1006 (1974).
- [34] J. Amar, F. Sullivan, and R. D. Mountain, *Phys. Rev. B* **37**, 196 (1988).
- [35] S. C. Glotzer, D. Stauffer, and N. Jan, *Phys. Rev. Lett.* **72**, 4109 (1994).
- [36] T. B. Liverpool, *Physica A* **224**, 589 (1996).
- [37] F. Mallamace, N. Micali, S. Trusso, and S. H. Chen, *Phys. Rev. E* **51**, 5818 (1995).